

SiO in C-rich circumstellar envelopes of AGB stars: effects of non-LTE chemistry and grain adsorption

F. L. Schöier¹, H. Olofsson^{1,2}, and A. A. Lundgren³

¹ Stockholm Observatory, AlbaNova University Center, SE-106 91 Stockholm, Sweden

² Onsala Space Observatory, SE-439 92 Onsala, Sweden

³ European Southern Observatory, Casilla 19001, Santiago 19, Chile

Received; accepted

Abstract. New SiO multi-transition millimetre line observations of a sample of carbon stars, including $J = 8 \rightarrow 7$ observations with the APEX telescope, are used to probe the role of non-equilibrium chemistry and the influence of grains in circumstellar envelopes of carbon stars. A detailed radiative transfer modelling, including the effect of dust emission in the excitation analysis, of the observed SiO line emission is performed. A combination of low- and high-energy lines are important in constraining the abundance distribution. It is found that the fractional abundance of SiO in these C-rich environments can be several orders of magnitude higher than predicted by equilibrium stellar atmosphere chemistry. In fact, the SiO abundance distribution of carbon stars closely mimic that of M-type (O-rich) AGB stars. A possible explanation for this behaviour is a shock-induced chemistry, but also the influence of dust grains, both as a source for depletion as well as production of SiO, needs to be further investigated. As observed for M-type AGB stars, a clear trend that the SiO fractional abundance decreases as the mass-loss rate of the star increases is found for the carbon stars. This indicates that SiO is accreted onto dust grains in the circumstellar envelopes.

Key words. Stars: AGB and post-AGB – Stars: carbon – Stars: circumstellar matter – Stars: late-type – Stars: mass-loss

1. Introduction

In addition to dictating the evolutionary time scale, stellar winds from late-type stars are thought to be important for the enrichment of heavy elements in the ISM (Gustafsson 2004). The stellar wind carries the results of internal nuclear processes, activated during evolution along the asymptotic giant branch (AGB), and thus contributes to the chemical evolution of galaxies.

Red giant stars located on the AGB divide into two chemically distinct groups; carbon stars ($C/O > 1$), which show a more rich chemistry than the M-type (O-rich) stars ($C/O < 1$). The molecular- and grain-type setups in the circumstellar envelopes (CSEs) around these mass losing stars are to a large extent determined by the C/O -ratio of the central star. Of paramount importance is to know how much of the elements that are eventually locked in dust particles and how much remains in the gas phase.

Observations of SiO line emission is particularly interesting because it is potentially a useful probe of the formation and evolution of dust grains in CSEs, as well as CSE dynamics: hinted at from early interferometric observations (Lucas et al. 1992; Sahai & Bieging 1993). A major survey of SiO emission from M-type AGB stars was performed by

González Delgado et al. (2003). Supplemented by a detailed numerical modelling of the detected radio line emission, they found that the circumstellar SiO fractional abundance (relative to H_2) for irregular and semi-regular variables in their sample had a median value of 5×10^{-6} , a factor of about ten lower than expected from theory (see, e.g., review by Millar 2003). For the high-mass-loss-rate Miras in their sample Gonzalez Delgado et al. found a distinct division into a low-abundance group (on average 4×10^{-7}) and a high-abundance group (on average 7×10^{-6}). They concluded that this division is not an effect of the modelling, but they found no obvious astrophysical explanation.

Interestingly, González Delgado et al. (2003) found a trend of decreasing circumstellar SiO fractional abundance with increasing mass-loss rate of the star, interpreted as an effect of increased adsorption of SiO onto dust grains with increasing mass-loss rate, i.e., the density of the envelope. This claim has been further corroborated by the recent interferometric SiO observations of the two low-mass-loss-rate M-type AGB stars R Dor and L² Pup performed by Schöier et al. (2004). The excitation analysis of these SiO ($\nu=0, J=2 \rightarrow 1$) interferometric observations requires the fractional abundance of SiO to be high, $\approx 4 \times 10^{-5}$, within $\approx 1 \times 10^{15}$ cm as suggested by stellar atmosphere models. Beyond this radius the SiO fractional abundance drops by about an order of magnitude and at $\approx 3 \times 10^{15}$ cm photodissociation destroys the SiO molecules. Thus, there

Send offprint requests to: F. L. Schöier
e-mail: fredrik@astro.su.se

Table 1. Integrated ($I_{\text{obs}} = \int T_{\text{mb}} dv$) line intensities in K km s⁻¹ for the new observations of SiO ($v = 0$, $J \rightarrow J - 1$) line emission.

Source ^a	OSO		NRAO		SEST			JCMT	APEX
	2 → 1	3 → 2	5 → 4	2 → 1	3 → 2	5 → 4	8 → 7	8 → 7	
LP And	0.94	0.62	2.76	
RV Aqr	3.87	
U Cam	1.20	...	
S Cep	...	1.26	
V Cyg	...	1.21	4.26	
R For	0.32 ^a	1.00	2.72	...	2.62	
V821 Her	4.97	
CW Leo	...	27.9	...	21.7	48.4	84.4	
R Lep	0.39 ^a	0.99	3.26	...	2.73	
RW LMi	3.45	1.82	4.49	
V384 Per	...	0.75	
W Pic	0.94;	
R Vol	0.67 ^a	1.04	
IRAS 07454–7112	5.12	
IRAS 15082–4808	8.51	
IRAS 15194–5115	20.4	

^a A colon (:) marks a low S/N detection.

^b Improved S/N-ratio compared to previous detection by Olofsson et al. (1998).

exists strong indications that the circumstellar SiO line emission carries information on the region where the mass loss is initiated, and where dust formation takes place.

In this paper we present new (sub-)millimetre line observations of SiO for a sample of carbon stars. The observations are supplemented by a detailed non-LTE radiative transfer analysis in order to obtain reliable circumstellar molecular abundances. The results are then compared to predictions from available chemical models and to the abundance estimates of SiO in M-type (oxygen-rich) AGB stars.

2. Observations

The observations were performed during 1994–1998 using the Onsala 20 m telescope¹ (OSO), the Swedish-ESO submillimetre telescope² (SEST), the NRAO 12 m telescope at Kitt Peak, in October 2003 using the JCMT telescope³, and in September 2005 using the APEX telescope⁴. The observed spectra are presented in Figs 1 & 2 and velocity-integrated intensities are re-

¹ The Onsala 20 m telescope is operated by the Swedish National Facility for Radio Astronomy, Onsala Space observatory at Chalmers University of technology

² The SEST was located on La Silla, Chile and operated jointly by the Swedish National Facility for Radio Astronomy and the European Southern Observatory (ESO).

³ Based on observations obtained with the James Clerk Maxwell Telescope, which is operated by the Joint Astronomy Centre in Hilo, Hawaii on behalf of the parent organizations PPARC in the United Kingdom, the National Research Council of Canada and The Netherlands Organization for Scientific Research

⁴ This publication is based on data acquired with the Atacama Pathfinder Experiment (APEX). APEX is a collaboration between the Max-Planck-Institut für Radioastronomie, the European Southern Observatory, and the Onsala Space Observatory

Table 2. Telescope data.

Transition	Frequency [GHz]	Telescope	η_{mb}	θ_{mb} ["]
$J = 2 \rightarrow 1$	86.847	SEST	0.75	57
		OSO	0.65	44
$J = 3 \rightarrow 2$	130.269	NRAO	0.80	49
		SEST	0.68	38
$J = 5 \rightarrow 4$	217.105	NRAO	0.55	29
		SEST	0.50	24
		JCMT	0.70	23
$J = 8 \rightarrow 7$	347.331	APEX	0.70	18
		JCMT	0.62	14

ported in Table 1. The intensity scales are given in main-beam brightness temperature scale (T_{mb}).

The SEST, OSO and JCMT observations were made in a dual beamswitch mode, where the source is alternately placed in the signal and the reference beam, using a beam throw of about 11' (SEST and OSO) or 2' (JCMT). This method produces very flat baselines. At the APEX 12 m telescope the observations were carried out using a position-switching mode, with the reference position located +2' in azimuth. The raw spectra are stored in the T_{A}^* scale and converted to main-beam brightness temperature using $T_{\text{mb}} = T_{\text{A}}^*/\eta_{\text{mb}}$. T_{A}^* is the antenna temperature corrected for atmospheric attenuation using the chopper-wheel method, and η_{mb} is the main-beam efficiency. Regular pointing checks were made on SiO masers (SEST and OSO) and strong CO sources (APEX) and typically found to be consistent within $\approx 3''$.

At the NRAO 12 m telescope the observations were carried out using a position-switching mode, with the reference posi-

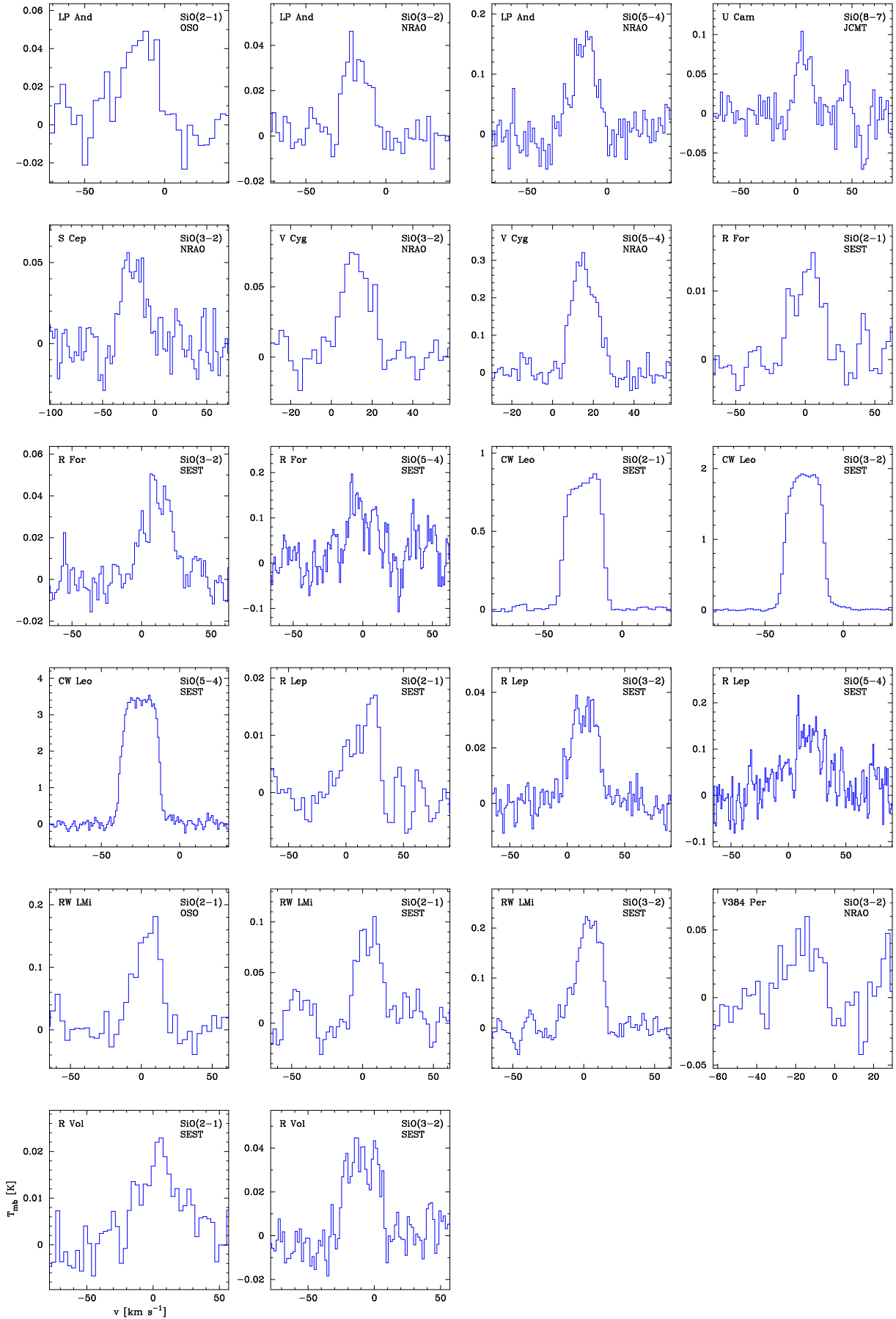


Fig. 1. New observations of SiO line emission.

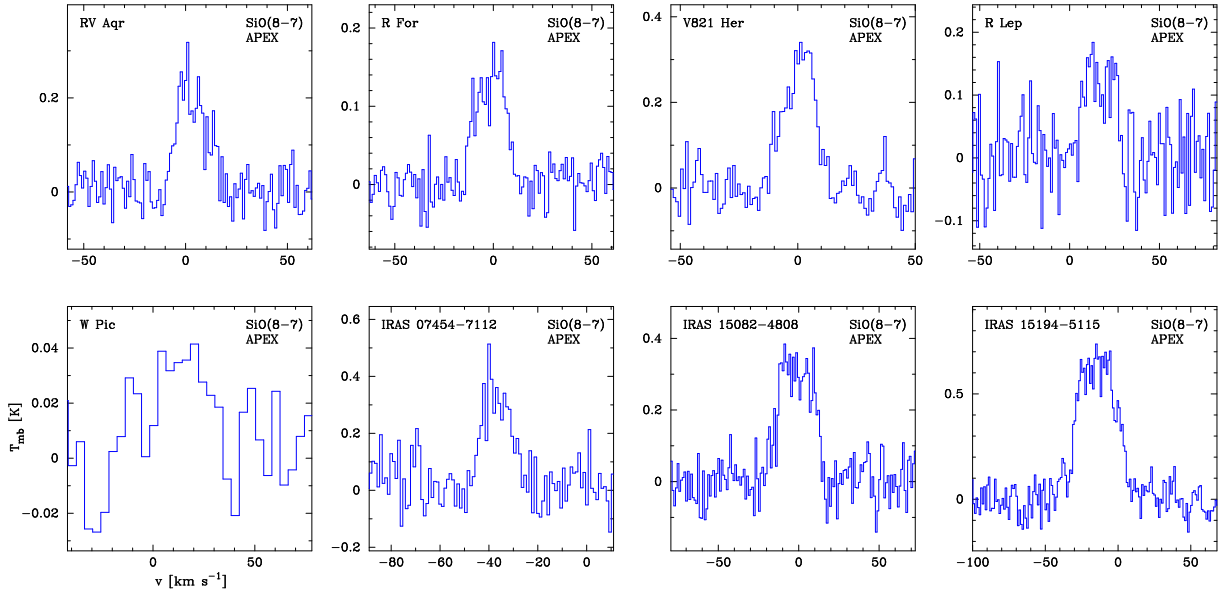


Fig. 2. New observations of SiO $J = 8 \rightarrow 7$ line emission using the APEX telescope. The velocity resolution is 1.0 km s^{-1} in all the spectra, except for W Pic which has been reduced to a resolution of 4.0 km s^{-1} .

tion located $+10'$ in azimuth. This is the preferred observation mode for spectral line observations at the 12 m telescope. The raw spectra, which are stored in the T_R^* scale, were converted using $T_{\text{mb}} = T_R^* / \eta_m^*$, where η_m^* is the corrected main-beam efficiency. The T_R^* scale is related to T_A^* through $T_R^* = T_A^* / \eta_{\text{fss}}$, where η_{fss} is the forward-scattering and spillover efficiency. Regular pointing checks were made on strong continuum sources and typically found to be consistent within $\approx 5''$.

The adopted beam efficiencies, together with the FWHM of the main beam (θ_{mb}), for all telescopes and frequencies are given in Table 2. The uncertainty in the absolute intensity scale is estimated to be about $\pm 20\%$.

The data was reduced in a standard way, by removing a low order baseline and then binned in order to improve the signal-to-noise ratio, using XS⁵.

In addition to the new data presented here we have also used SiO line intensities reported by Olofsson et al. (1982, 1998) & Woods et al. (2003) ($J=2 \rightarrow 1$), Bujarrabal et al. (1994) ($J=2 \rightarrow 1$ and $3 \rightarrow 2$), and Bieging et al. (2000) ($J=5 \rightarrow 4$ and $8 \rightarrow 7$). In total, 19 carbon stars have been detected in SiO line emission.

These stars detected in SiO millimetre line emission provide our sample and are listed in Table 3.

3. Molecular excitation analysis

3.1. Radiative transfer model

The CSEs are assumed to be spherically symmetric, produced by a constant mass loss rate (\dot{M}), and to expand at a constant velocity (v_e). In order to determine the molecular excitation in the CSEs a detailed non-LTE radiative transfer code, based

⁵ XS is a package developed by P. Bergman to reduce and analyse a large number of single-dish spectra. It is publically available from <ftp://yggdrasil.oso.chalmers.se>

on the Monte Carlo method, was used. The code is described in detail in Schöier & Olofsson (2001) and has been benchmarked, to high accuracy, against a wide variety of molecular-line radiative transfer codes in van Zadelhoff et al. (2002) and van der Tak et al. (in prep.).

Schöier & Olofsson (2001) set out to determine the circumstellar physical properties, such as the density, temperature, and kinematic structures, of a large sample of carbon stars based on radiative transfer modelling of millimetre CO line observations. These models, and subsequent models presented in Schöier et al. (2002) and Woods et al. (2003), form the basis of the underlying physical structure and are used as input to the SiO excitation analysis. In a similar way new circumstellar models were obtained for V821 Her (IRAS 18397+1738) and V1965 Cyg (IRAS 19321+2757) using CO millimetre line observations published in Margulis et al. (1990), Nyman et al. (1992), and from the JCMT data archive⁶.

The local line width is assumed to be described by a Gaussian and is made up of a micro-turbulent component and a thermal component. The micro-turbulence is assumed to have a width of 1.0 km s^{-1} (Schöier et al. 2004). This is significantly higher than the value of 0.5 km s^{-1} adopted in the CO modelling performed by Schöier & Olofsson (2001). However, as pointed out by Schöier & Olofsson the exact value adopted for the micro-turbulence only has a minor effect on the derived mass-loss rates, as long as it is much lower than the expansion velocity of the wind. The (sub)millimetre SiO observations typically probe regions of gas closer to the star than does the CO sub(millimetre) observations. Observations of IR-absorption lines (Monnier et al. 2000) indicate that most likely there is a gradient in turbulent velocity, with regions closer to the photosphere being more turbulent. Thus, it is not unreasonable to adopt a higher turbulent velocity when modelling the

⁶ <http://www.jach.hawaii.edu/JCMT/archive/>.

Table 3. Model results.

Source	SED modelling								CO modelling				SiO modelling			
	D [pc]	L_\star [L_\odot]	T_\star [K]	τ_{10}	T_c [K]	r_i [cm]	χ^2_{red}	N	\dot{M} [$M_\odot \text{ yr}^{-1}$]	v_e [km s^{-1}]	χ^2_{red}	N	f_0	r_e [cm]	χ^2_{red}	N
LP And	630	9400	2000	0.60	1100	1.8×10^{14}	0.8	11	1.5×10^{-5}	13.5	0.7	7	1.2×10^{-7}	2.2×10^{16}	2.9	3
RV Aqr	670	6800	2200	0.27	1300	7.6×10^{13}	0.8	9	2.8×10^{-6}	15.0	0.3	3	4.0×10^{-6}	9.3×10^{15}	0.1	2
UU Aur	260	6900	2800	0.017	1500	6.3×10^{13}	1.3	9	2.4×10^{-7}	10.5	1.0	5	1.0×10^{-6}	3.4×10^{15}	...	1
U Cam ^a	340	7000	2700	0.01	1500	4.4×10^{13}	1.5	9	2.0×10^{-7}	11.5	...	4	5.0×10^{-5}	3.0×10^{15}	...	1
S Cep	380	7300	2200	0.12	1400	5.8×10^{13}	1.5	9	1.2×10^{-6}	21.5	0.9	5	9.0×10^{-6}	4.8×10^{15}	0.4	4
V Cyg	310	6300	1900	0.08	1200	8.7×10^{13}	0.6	8	9.0×10^{-7}	10.5	0.5	5	3.5×10^{-6}	6.4×10^{15}	3.0	6
V1965 Cyg	1200	9800	2000	0.55	1000	2.2×10^{14}	1.1	10	1.0×10^{-5}	27.0	2.0	3	7.0×10^{-6}	1.4×10^{16}	...	1
R For	610	5800	2000	0.25	1400	5.6×10^{13}	2.8	9	1.1×10^{-6}	16.0	1.5	7	8.0×10^{-6}	5.8×10^{15}	0.3	4
V821 Her	600	7900	2200	0.45	1500	8.1×10^{13}	2.4	10	1.8×10^{-6}	13.0	3.9	4	6.0×10^{-6}	8.1×10^{15}	0.1	2
CW Leo	120	9600	2000	0.90	1200	1.7×10^{14}	2.1	9	1.5×10^{-5}	14.0	0.5	8	2.0×10^{-7}	2.2×10^{16}	1.0	9
R Lep	250	4000	2200	0.06	1500	4.3×10^{13}	0.3	9	5.0×10^{-7}	16.5	0.7	6	2.8×10^{-6}	4.5×10^{15}	0.9	4
RW LMi	440	9700	2000	0.50	1000	2.1×10^{14}	1.4	11	6.0×10^{-6}	16.5	1.1	7	2.0×10^{-6}	1.3×10^{16}	1.5	5
V384 Per	560	8100	2000	0.25	1300	1.0×10^{14}	1.5	11	3.5×10^{-6}	14.5	0.7	6	1.5×10^{-6}	1.1×10^{16}	3.2	3
W Pic	490	4000	2500	0.015	1500	4.5×10^{13}	3.2	8	2.3×10^{-7}	15.0	3.4	3	1.9×10^{-5}	2.8×10^{15}	...	1
R Vol	730	6800	2000	0.30	1500	6.6×10^{13}	1.1	9	1.7×10^{-6}	16.5	0.6	3	9.0×10^{-6}	7.0×10^{15}	1.5	2
AFGL 3068	980	7800	2000	2.70	1100	2.5×10^{14}	1.8	8	1.0×10^{-5}	13.5	0.6	4	2.0×10^{-7}	1.8×10^{16}	...	1
IRAS 07454–7112	710	9000	2100	0.45	1200	1.4×10^{14}	1.0	9	5.0×10^{-6}	12.5	0.1	2	1.3×10^{-6}	1.3×10^{16}	0.3	2
IRAS 15082–4808	640	9000	2200	0.80	1100	1.9×10^{14}	7.0	9	1.0×10^{-5}	19.0	0.2	2	1.8×10^{-6}	1.5×10^{16}	2.3	2
IRAS 15194–5115	500	8800	2400	0.55	1200	1.5×10^{14}	0.4	9	9.0×10^{-6}	21.0	0.9	4	5.0×10^{-6}	1.4×10^{16}	1.9	2

^a U Cam has a detached shell that complicates the analysis of the present-day mass-loss characteristics (for details see Schöier et al. 2005a). A colon (:) marks an uncertain abundance estimate.

SiO line emission. The thermal line broadening is calculated from the derived kinetic temperature structure.

Since the publication of Schöier & Olofsson (2001) new collisional rate coefficients of CO have been calculated by Flower (2001). These new rate coefficients were adopted here and extended to include more energy levels as well as extrapolated in temperature, as described in Schöier et al. (2005b). An ortho-to-para ratio of 3.0 was adopted when weighting together collisional rate coefficients for CO in collisions with ortho-H₂ and para-H₂. In addition, dust emission has been included in the excitation analysis for CO in the same fashion as for SiO described below. Moreover, new CO observations of $J = 3 \rightarrow 2$ line emission using the JCMT and APEX telescopes (Schöier & Olofsson, in prep.) has been included in the modelling. In all, these new modifications to the excitation analysis of CO millimetre line emission have not altered the mass-loss rates derived by Schöier & Olofsson (2001) by more than 20%, i.e., within the calibration uncertainty of the observations. The new mass-loss rates are reported in Table 3.

The excitation analysis includes radiative excitation through the first vibrationally excited ($\nu = 1$) state for both CO at $4.6 \mu\text{m}$ and SiO at $8 \mu\text{m}$. Relevant molecular data are summarized in Schöier et al. (2005b) and are made publicly available through the *Leiden Atomic and Molecular Database* (LAMDA)⁷. The majority of sources in this study are intermediate- to high-mass-loss-rate objects where thermal

dust emission provides the main source of infrared photons which excite the $\nu = 1$ state.

The addition of a dust component in the Monte Carlo scheme is straightforward as described in Schöier et al. (2002). At the wavelengths of importance here ($\lambda \geq 4.8 \mu\text{m}$) scattering can be neglected and only emission and absorption by the dust particles need to be considered. The number of model photons emitted per second by the dust within a small volume of the envelope, ΔV , and over a small frequency interval, $\Delta \nu$, can then be written as

$$N_d(r) = \frac{4\pi}{h\nu} \kappa_\nu \rho_d(r) B_\nu [T_d(r)] \Delta V(r) \Delta \nu, \quad (1)$$

where κ_ν is the dust opacity per unit mass, ρ_d the dust mass density, and B_ν the Planck function. $T_d(r)$ is the temperature of the thermally emitting dust grains. Typically, the frequency passband corresponds to $3 \times \nu_e$ and it is centered on the line rest frequency ν_0 .

The model photons emitted by the dust are released together with the other model photons. The additional opacity provided by the dust,

$$\tau_\nu = \kappa_\nu \int \rho_d(r) dr, \quad (2)$$

is added to the line optical depth.

3.2. SED modelling

The dust-temperature structure and dust-density profile are obtained from detailed radiative transfer modelling using *Dusty*

⁷ <http://www.strw.leidenuniv.nl/~moldata>

(Ivezić & Elitzur 1997). Here we are only interested in the potential of dust grains to affect the excitation of molecules. A full treatment of dust radiative transfer coupled with a dynamical model for the wind, in order to independently measure physical properties of the CSE such as, e.g., the mass-loss rate, is beyond the scope of this paper and left to a future publication (Schöier & Olofsson, in prep.). In the dust modelling the same basic assumptions are made as for the gas modelling, i.e., a spherically symmetric envelope expanding at a constant velocity. Prompt dust formation is assumed at the inner radius, r_i , of the CSE. Amorphous carbon dust grains with the optical constants given in Suh (2000) are adopted. For simplicity, the dust grains are assumed to be of the same size (a radius, a_d , of $0.1 \mu\text{m}$), and the same mass density ($\rho_s = 2.0 \text{ g cm}^{-3}$). The corresponding dust opacities, κ_ν , were then calculated from the optical constants and the individual grain properties using standard Mie theory (Bohren & Huffman 1983).

In the modelling, where the SED provides the observational constraint, the dust optical depth specified at $10 \mu\text{m}$, τ_{10} , and the dust condensation temperature, $T_d(r_i)$, are the adjustable parameters in the χ^2 -analysis. The model SED only weakly depends on the other input parameters which are fixed at reasonable values. The SED typically consists of *JHKLM* photometric data (Kerschbaum 1999, and Kerschbaum priv. com.), IRAS fluxes, and in some cases submillimetre data (Groenewegen et al. 1993). The total luminosity of the source is obtained from the period-luminosity relation of Groenewegen & Whitelock (1996). The distance is then obtained from the SED fitting. The derived parameters are reported in Table 3 and examples of best-fit models are shown in Fig. 3 for the new sample sources V821 Her and V1965 Cyg. A more detailed description of the procedure as well as other examples for the sample stars can be found in Schöier et al. (2002).

3.3. SiO envelope sizes

In order to determine accurate abundances it is important to know the spatial extent of the molecules. González Delgado et al. (2003) showed that it is possible to put constraints also on the size of the SiO line emitting envelope from single-dish observations alone, given that enough transitions are observed (in practice four or more). In the present sample six carbon stars (CW Leo, R For, R Lep, RW LMi, S Cep, and V Cyg) have been observed in four or more transitions. For these sources the size of the SiO emitting region (r_e) and the inner fractional abundance of SiO (f_0) are varied simultaneously. The abundance distribution is assumed to be described by a Gaussian

$$f(r) = f_0 \exp\left(-\left(\frac{r}{r_e}\right)^2\right), \quad (3)$$

where $f = n(\text{SiO})/n(\text{H}_2)$, i.e., the ratio of the number density of SiO molecules to that of H_2 molecules. In circumstellar envelopes such as these H is expected to be mainly in molecular form.

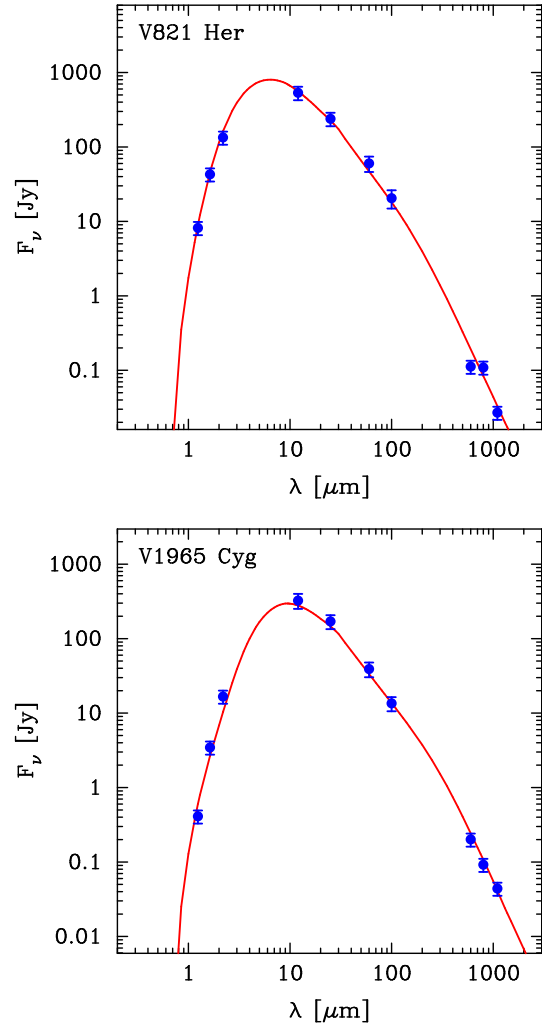


Fig. 3. Best-fit models, derived from the dust radiative transfer modelling (parameters given in Table 3), of the observed SEDs for V821 Her and V1965 Cyg.

The best fit model is found by minimizing the total χ^2 defined as

$$\chi_{\text{tot}}^2 = \sum_{i=1}^N \left[\frac{(I_{\text{mod}} - I_{\text{obs}})}{\sigma} \right]^2, \quad (4)$$

where I is the integrated line intensity and σ the uncertainty in the measured value (usually dominated by the calibration uncertainty of $\pm 20\%$), and the summation is done over N independent observations. The sensitivity of the line emission to variations of the two adjustable parameters r_e and f_0 is illustrated in Fig. 4. As can be seen reasonable estimates can be found for all four objects, also the quality of the best-fit models are good, typically $\chi_{\text{red}}^2 = \chi_{\text{tot}}^2 / (N - 2) \sim 1$. The 1σ range of acceptable values for r_e and f_0 are reported in Table 4. However, note that the range of acceptable values does not follow a rectangular shape as seen in Fig. 4.

Given the relatively low number of carbon stars where r_e can be determined we have assumed it to scale with density as

$$\log r_e = 19.2 + 0.48 \log \left(\frac{\dot{M}}{v_e} \right), \quad (5)$$

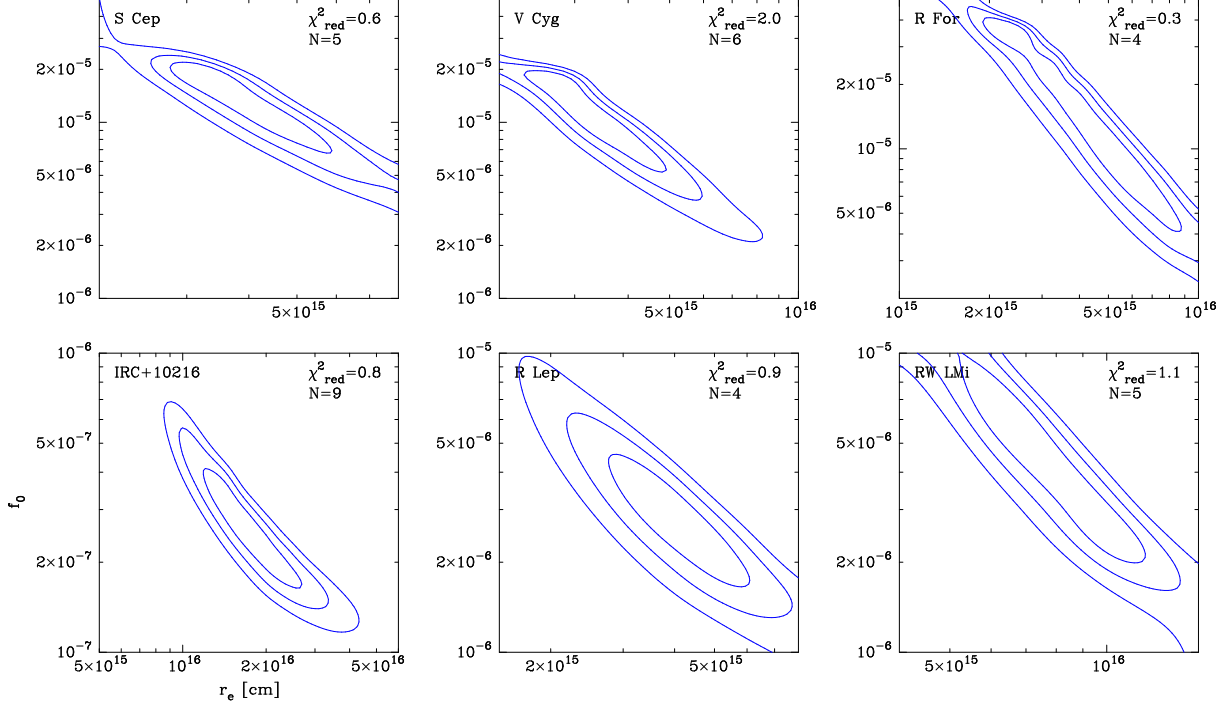


Fig. 4. χ^2 maps showing the sensitivity of the excitation analysis to the adopted SiO fractional abundance (f_0) and envelope size (r_e). Contours are drawn at the 1, 2, and 3σ levels. Also indicated is the lowest reduced χ^2 ($\chi^2_{\text{red}} = \chi^2_{\text{tot}}/(N - 2)$) in the map.

Table 4. SiO abundance distribution.

Source	f_0^a	r_e^a [cm]	N	χ^2_{red}
S Cep	$1.4 \pm 0.8 \times 10^{-5}$	$4.4 \pm 1.6 \times 10^{15}$	5	0.6
V Cyg	$1.3 \pm 0.7 \times 10^{-5}$	$3.6 \pm 1.3 \times 10^{15}$	6	2.0
R For	$2.2 \pm 1.8 \times 10^{-5}$	$5.4 \pm 3.6 \times 10^{15}$	4	0.3
CW Leo	$2.8 \pm 1.1 \times 10^{-7}$	$1.9 \pm 0.7 \times 10^{16}$	9	0.8
R Lep	$3.1 \pm 1.4 \times 10^{-6}$	$4.4 \pm 1.6 \times 10^{15}$	4	0.9
RW LMi	$6.0 \pm 4.0 \times 10^{-6}$	$7.7 \pm 2.5 \times 10^{15}$	5	1.1

^a The abundance distribution is assumed to be Gaussian (see Eq. 3)

where \dot{M} is the mass-loss rate and v_e is the expansion velocity of the wind. This scaling law was found by González Delgado et al. (2003) for a larger sample of M-type AGB stars. As shown in Fig. 5 this scaling law can, within the uncertainties, account for the estimated envelope sizes derived for the carbon stars in our study.

The radial distribution of SiO molecules in the gas-phase is most probably determined by a combination of condensation and photodissociation processes. Thus, one can imagine an initial (pre-condensation) SiO abundance determined by the stellar atmosphere chemistry, possibly modified by non-LTE chemical processes due to shocks in the inner part of the wind out to a few stellar radii (e.g., Willacy & Cherchneff 1998). In terms of classical evaporation theory (see González Delgado et al. 2003, and references therein) the region over which the SiO abundance is expected to change significantly due to condensation onto dust grains is confined within approximately 10^{15} cm. For intermediate- to

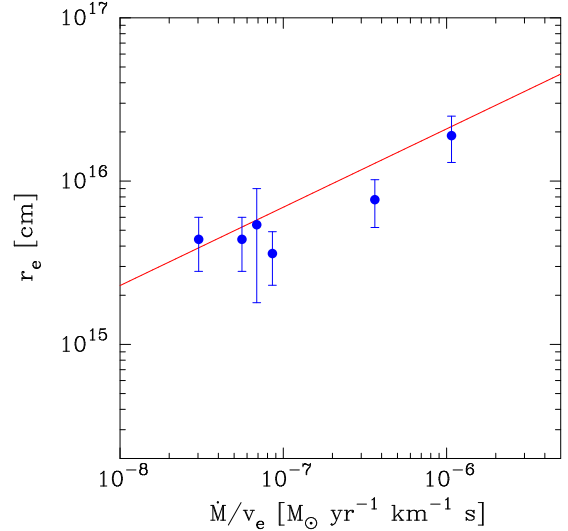


Fig. 5. SiO envelope sizes (r_e) estimated from the excitation analysis plotted against a density measure (\dot{M}/v_e). The solid line is the relation found for a larger sample of M-type AGB stars (Eq. 5).

high-mass-loss-rate objects this region is significantly smaller than the post-condensation region (see Fig. 5), which is limited by photodissociation, and it does not contribute notably to the observed single-dish fluxes. Thus, a single component is adequate for describing the SiO abundance structure in this case. It should be pointed out that this also means that no constraints can be put on the pre-condensation abundance from the present observations. This requires high spatial resolution observations (Schöier et al. 2004). In the case of low-mass-loss-

rate objects the post-condensation region is smaller, but, since the freeze out is less effective, the contrast between pre- and post-condensation SiO abundances is small. Hence, a single component description is adequate also in this case.

3.4. SiO abundances

Using the scaling relation in Eq. 5 it is possible to estimate the characteristic size of the envelope (r_e) containing SiO molecules for each of the sample sources. Once the size is known only one free parameter remains, the fractional abundance of SiO (f_0). The derived sizes and abundances are reported in Table 3. The fits are generally excellent with reduced χ^2 values of $\approx 1-2$. As examples we show the best-fit models for R For and R Lep in Fig. 6.

From the modelling it is noted that the SiO $J = 3 \rightarrow 2$ line observed using the IRAM 30 m telescope by Bujarrabal et al. (1994) is consistently lower by about a factor of two compared to model predictions. A possible explanation for this is pointing offsets on the order of $\approx 8''$. Due to the larger beam the $J = 2 \rightarrow 1$ observations are less affected, typically on the same level as the absolute calibration uncertainty $\approx 20\%$. However a calibration error can not be ruled out. In the present analysis the SiO $J = 3 \rightarrow 2$ line intensities reported by Bujarrabal et al. (1994) were not included, except for UU Aur which is only detected in this line.

Making an error estimate of the derived abundance is difficult as discussed in González Delgado et al. (2003). We have also tested the effect of the assumed abundance distribution by replacing the adopted Gaussian distribution (Eq. 3) by an exponential decline of the abundance, $f(r) = f_0 \exp(-r/r_e)$, as would be the case for a simple photodissociation model without any dust shielding. In the case of a high-mass-loss-rate object such as CW Leo the line intensities change by $\lesssim 5\%$ and for a low-mass-loss-rate object such as R Lep by $\lesssim 20\%$. Thus, no significant systematic trends are introduced through the choice of the SiO abundance description. Typically, we believe the abundances to be accurate to about $\pm 50\%$, within the adopted circumstellar model.

3.5. Importance of vibrational excitation

The excitation analysis includes the possibility of populating also the first vibrationally-excited state of SiO through the absorption of $8\mu\text{m}$ photons, primarily, from dust emission. This can significantly change the derived line intensities of transitions within the ground vibrational state as illustrated in Table 5 for CW Leo (and R Lep) for selected transitions. The calculations were performed for a 15 m telescope. Neglecting to take account of the dust leads to about 50% lower integrated (over the line) intensities, which translates into at least a doubled fractional abundance of circumstellar SiO to produce the same flux. Interestingly, in this example approximating the dust emission using a single low-temperature ($T = 510\text{ K}$) blackbody containing the total luminosity of the source produces only about 10% higher intensities compared with the full model taking the dust emission/absorption fully into account. This is

Table 5. Importance of IR pumping in the excitation of SiO.

Model with	$I(2 \rightarrow 1)$ [K km s ⁻¹]	$I(3 \rightarrow 2)$ [K km s ⁻¹]	$I(5 \rightarrow 4)$ [K km s ⁻¹]	$I(8 \rightarrow 7)$ [K km s ⁻¹]
<i>CW Leo</i>				
no (star + dust)	11.2	22.8	41.1	74.3
star	13.1	28.0	46.8	81.0
star + dust	16.5	47.3	98.9	159.2
510 K BB	20.4	51.5	100.3	172.6
<i>R Lep</i>				
no (star + dust)	0.27	0.60	1.1	2.0
star	0.34	0.88	1.7	2.8
star + dust	0.34	1.08	2.6	4.5

not always the case and great caution should be taken when such approximations are made. It should be noted that CW Leo is a high-mass-loss-rate object and that the importance of the circumstellar dust radiation in relation to that of the stellar radiation field is less for a lower-mass-loss-rate object such as R Lep (Table 5).

4. Discussion

4.1. Comparison with chemical models

LTE stellar atmosphere models predict that the SiO fractional abundance in carbon stars is relatively low, typically $\sim 5 \times 10^{-8}$ (see reviews by Glassgold 1999; Millar 2003, and references therein) about three orders of magnitudes lower than in M-type AGB stars. The relatively high SiO fractional abundances, derived in Sect. 3, of $1 \times 10^{-7} - 5 \times 10^{-5}$ can generally not be explained by LTE chemistry.

Departure from LTE could be caused by the variable nature of AGB stars that induces shocks propagating through the photosphere thereby affecting its chemistry. Models of shocked carbon-rich stellar atmospheres performed by Willacy & Cherchneff (1998) and Helling & Winters (2001) indicate that the SiO fractional abundance can be significantly increased by the passage of periodic shocks. There is also a strong dependence on the shock strength and possibly this mechanism can explain the observed fractional abundances, and their large spread, of SiO in carbon stars.

From the results reported in Table 3 it is clear that the fractional abundance of SiO varies substantially between the carbon stars in the sample, from as low as 1×10^{-7} up to 5×10^{-5} . As illustrated in Fig. 7 (solid circles) there is a clear trend that SiO becomes less abundant as the density, \dot{M}/v_e , in the wind increases. Even more intriguing, when compared to the distribution of SiO fractional abundances for M-type AGB stars derived by González Delgado et al. (2003) (Fig. 7; filled squares), there appears to be no way of distinguishing a C-rich chemistry from that of an O-rich based on an estimate of the circumstellar SiO abundance alone. Also, the puzzling division of high-mass-loss-rate stars, into distinct low- and high-SiO fractional abundance groups, found by González Delgado et al. (2003) for M-

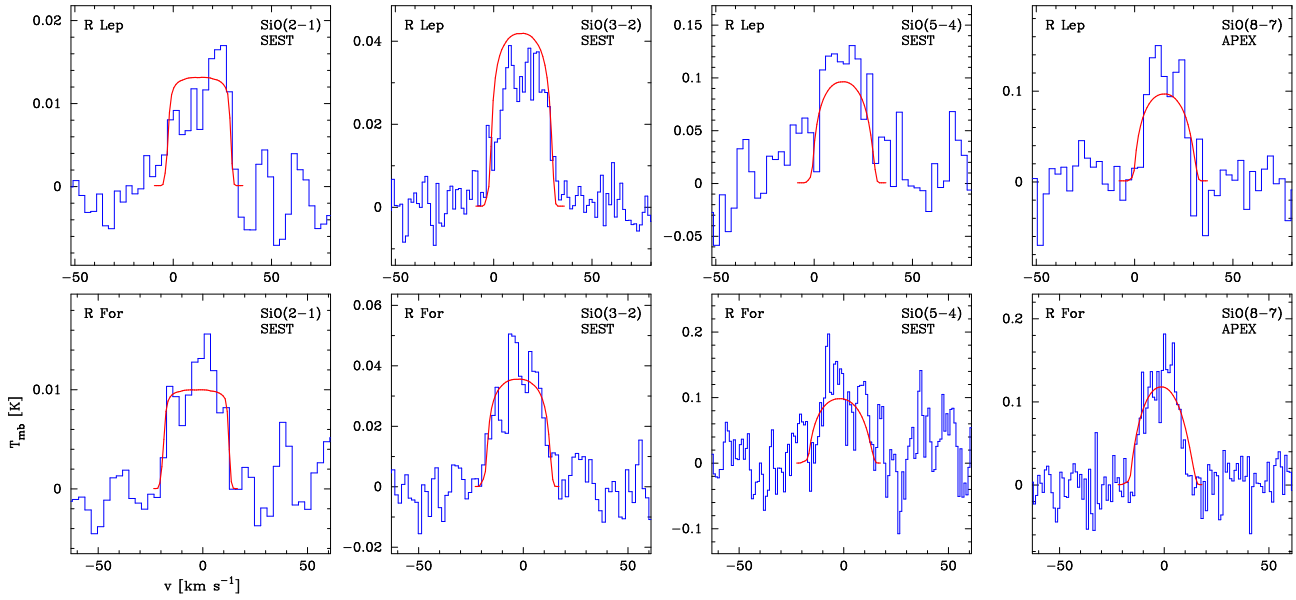


Fig. 6. Best-fit models (solid lines; parameters given in Table 3) for R Lep and R For overlaid on observed spectra (histograms).

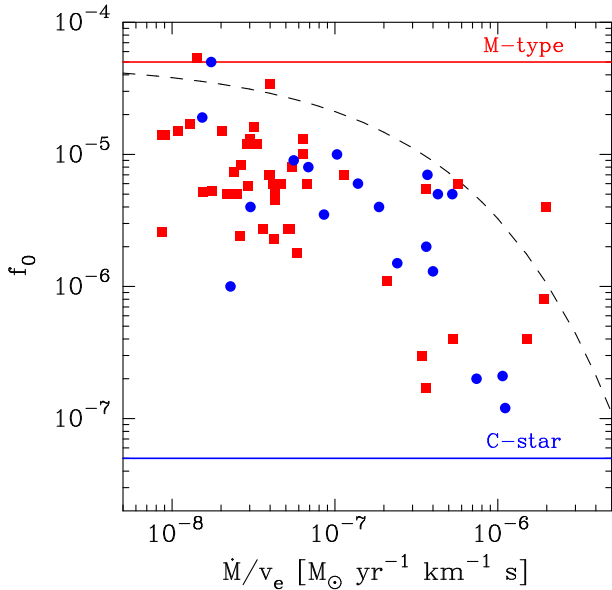


Fig. 7. SiO fractional abundance (f_0) obtained from an excitation analysis, as a function of a density measure (\dot{M}/v_e), for carbon stars (filled circles) and M-type (O-rich) AGB stars (filled squares). The horizontal lines mark the abundances predicted from equilibrium chemistries. The dashed line shows the expected $f(\infty)$ (scaled to 5×10^{-5} , roughly the expected fractional abundance from stellar equilibrium chemistry when $C/O < 1$) for a model including adsorption of SiO onto dust grains (see González Delgado et al. 2003, for details).

type stars is reinforced by the excitation analysis of the carbon stars.

The non-detection of SiO maser emission (e.g., from the $\nu = 1$, $J = 2 \rightarrow 1$ transition) towards carbon stars (e.g., Lepine et al. 1978) is interesting in light of the high circumstellar SiO abundances found. Since SiO maser emission detected

from M-type AGB stars emanates very close to the photosphere and well within the acceleration region (e.g., Cotton et al. 2004) this could suggest that in carbon stars the SiO molecules form somewhat further out in the wind where pumping by IR photons, and hence excitation of vibrationally excited states, is less effective.

4.2. Condensation onto dust grains

The importance of dust grains in regulating the circumstellar fractional abundance of SiO is supported by the observed trend that the SiO fractional abundance decreases with increasing density (\dot{M}/v_e) of the wind (Fig. 7). This trend is expected from a classical treatment of the condensation process, as described in González Delgado et al. (2003), where the condensation efficiency strongly depends on the dust mass-loss rate. In Fig. 7 a depletion curve based on the simple model presented in González Delgado et al. (2003) is shown. Since the theoretical condensation results are very sensitive to the adopted parameters a large scatter around this curve is natural.

In Fig. 7 the derived abundances are plotted against a density measure where the terminal expansion velocity of the wind has been used. Since much of the condensation may occur in the acceleration region a lower velocity (and hence a higher density) is perhaps more suitable. However, if the characteristic velocity at which dust condensation is close to complete scales with the terminal expansion velocity (independently of the mass-loss rate), the results would only be shifted along the density axis in Fig. 7. If, on the other hand, this velocity is independent of the mass-loss rate plotting the abundance against the mass-loss rate is to be preferred. However, this only marginally changes the appearance of Fig. 7 (see also Fig. 5 in González Delgado et al. 2003).

The inclusion of adsorption of molecules onto dust grains is a shortcoming of current generation chemical models and will be required in a full model describing the chemistry of

AGB stars. In addition, grain surfaces could act as catalysts for chemical reactions. Although LTE chemistry can explain the SiO fractional abundances for a few of the carbon stars with the highest mass-loss rates we find it more likely that these abundances are the result of SiO depletion in the wind and that the photospheric abundance is significantly higher. High spatial resolution interferometric observations for a sample of sources could help to solidify this claim.

4.3. The HCN/SiO line intensity ratio

The HCN/SiO line intensity ratio has been shown to be a useful tool to discriminate between O-rich and C-rich envelopes (Bujarrabal et al. 1994; Olofsson et al. 1998; Bieging et al. 2000). The explanation for this has been that in O-rich envelopes the abundance of HCN is very low and that of SiO high, naturally producing a low HCN/SiO line-intensity ratio. In a C-rich envelope HCN is abundant whereas SiO is not, producing a high HCN/SiO line-intensity ratio. Caution has to be taken here since optical depth effects are present, in particular for high-mass-loss-rate objects.

From the present analysis it is suggested that the SiO fractional abundance in carbon stars closely mimic that in M-type (O-rich) stars. Therefore, we conclude that the observed difference in the HCN/SiO line intensity ratio of about an order of magnitude is mainly due to a significantly lower fractional abundance of HCN in M-type AGB stars compared with the carbon stars. This claim has to be verified by performing a similar excitation analysis, as presented for SiO here and in González Delgado et al. (2003), also for a statistically significant sample of sources detected in HCN line emission.

5. Conclusions

New multi-transition millimetre SiO line observations of a sample of carbon stars are presented. With this addition, a total of 19 carbon stars have been detected in SiO line emission. From a detailed excitation analysis, based on a reliable physical model of the sources, we reach the following conclusions:

- In order to derive reliable fractional abundances of SiO, excitation through IR ro-vibrational transitions, needs to be taken into account. This will in most cases mean that the effect of dust grains need to be included in the excitation analysis. The present work contains a proper treatment of this.
- The fractional abundance of SiO in carbon stars can be several orders of magnitude higher than predicted by thermal equilibrium chemistry.
- A possible explanation for the high SiO fractional abundances found is a shock-induced chemistry. However, the influence of dust grains, both as a source for depletion as well as production of SiO, needs to be further investigated.
- As observed for M-type AGB stars, a clear trend that the SiO fractional abundance in carbon stars decreases as the density (\dot{M}/v_e) of the wind increases is found, indicative of adsorption of SiO onto dust grains.

However, these conclusions still rest on somewhat loose ground, e.g., the constraints on the SiO abundance distribution are poor, and the relative importance of freeze-out onto dust grains, photodissociation, and circumstellar chemistry is still uncertain. More observations are required, in particular interferometric observations and high- J single dish observations, to more firmly establish these claims. Also, a larger number of low-mass-loss-rate carbon stars must be observed with high sensitivity.

Acknowledgements. The authors are grateful to the staff at the APEX telescope. An anonymous referee is thanked for insightful comments. FLS and HO acknowledge financial support from the Swedish Research Council.

References

- Bieging, J. H., Shaked, S., & Gensheimer, P. D. 2000, *ApJ*, 543, 897
- Bohren, C. F. & Huffman, D. R. 1983, *Absorption and scattering of light by small particles* (New York: Wiley, 1983)
- Bujarrabal, V., Fuente, A., & Omont, A. 1994, *A&A*, 285, 247
- Cotton, W. D., Mennesson, B., Diamond, P. J., et al. 2004, *A&A*, 414, 275
- Flower, D. R. 2001, *J. Phys. B.*, 34, 2731
- Glassgold, A. E. 1999, in *IAU Symp. 191: Asymptotic Giant Branch Stars*, 337
- González Delgado, D., Olofsson, H., Kerschbaum, F., et al. 2003, *A&A*, 411, 123
- Groenewegen, M. A. T., de Jong, T., & Baas, F. 1993, *A&AS*, 101, 513
- Groenewegen, M. A. T. & Whitelock, P. A. 1996, *MNRAS*, 281, 1347
- Gustafsson, B. 2004, in *EAS Publications Series*, 21–50
- Helling, C. & Winters, J. M. 2001, *A&A*, 366, 229
- Ivezić, Ž. & Elitzur, M. 1997, *MNRAS*, 287, 799
- Kerschbaum, F. 1999, *A&A*, 351, 627
- Lepine, J. R. D., Scalise, E., & Le Squeren, A. M. 1978, *ApJ*, 225, 869
- Lucas, R., Bujarrabal, V., Guilloteau, S., et al. 1992, *A&A*, 262, 491
- Margulis, M., van Blerkom, D. J., Snell, R. L., & Kleinmann, S. G. 1990, *ApJ*, 361, 673
- Millar, J. 2003, in *Asymptotic giant branch stars*, ed. H. J. Habing & H. Olofsson (Astronomy and astrophysics library, New York, Berlin: Springer), 247
- Monnier, J. D., Danchi, W. C., Hale, D. S., Tuthill, P. G., & Townes, C. H. 2000, *ApJ*, 543, 868
- Nyman, L.-Å., Booth, R. S., Carlstrom, U., et al. 1992, *A&AS*, 93, 121
- Olofsson, H., Johansson, L. E. B., Hjalmarsen, A., & Nguyen-Quang-Rieu, M. 1982, *A&A*, 107, 128
- Olofsson, H., Lindqvist, M., Nyman, L.-Å., & Winnberg, A. 1998, *A&A*, 329, 1059
- Sahai, R. & Bieging, J. H. 1993, *AJ*, 105, 595
- Schöier, F. L., Lindqvist, M., & Olofsson, H. 2005a, *A&A*, 436, 633
- Schöier, F. L. & Olofsson, H. 2001, *A&A*, 368, 969

- Schöier, F. L., Olofsson, H., Wong, T., Lindqvist, M., & Kerschbaum, F. 2004, *A&A*, 422, 651
- Schöier, F. L., Ryde, N., & Olofsson, H. 2002, *A&A*, 391, 577
- Schöier, F. L., van der Tak, F. F. S., van Dishoeck, E. F., & Black, J. H. 2005b, *A&A*, 432, 369
- Suh, K. 2000, *MNRAS*, 315, 740
- van Zadelhoff, G.-J., Dullemond, C. P., van der Tak, F. F. S., et al. 2002, *A&A*, 395, 373
- Willacy, K. & Cherchneff, I. 1998, *A&A*, 330, 676
- Woods, P. M., Schöier, F. L., Nyman, L.-Å., & Olofsson, H. 2003, *A&A*, 402, 617